Turkish Journal of Chemistry

Volume 46 | Number 4 Article 31

1-1-2022

A facile synthesis of Ag_2MnSnS_4 nanorods through colloidal method

SULTAN SÜLEYMAN ÖZEL

SERDAR AKAY

FARUK ÖZEL

Turkish Journal of Chemistry

http://journals.tubitak.gov.tr/chem/

Research Article

Turk J Chem
(2022) 46: 1291-1296

doi:10.55730/1300-0527.3435

A facile synthesis of Ag_2MnSnS_4 nanorods through colloidal method

Sultan Süleyman ÖZEL[1], Serdar AKAY[2], Faruk ÖZEL[3,*]

[1]Department of Materials Science and Engineering, Erciyes University, Kayseri, Turkey
[2]Department of Industrial Product Development, Production, and Design, Jönköping University, Jönköping, Sweden
[3]Department of Metallurgical and Materials Engineering, Karamanoğlu Mehmetbey University, Karaman, Turkey

Received: 13.12.2021 • **Accepted/Published Online:** 28.04.2022 • **Final Version:** 05.08.2022

Abstract: The production methods of semiconductor nanomaterials with new shapes and different compositions form the basis for the creation of high-performance structures in numerous applications. Kesterite structured materials are among these inorganic semiconductors and are suggested to be promising energy materials for the future. In this study, quaternary Ag_2MnSnS_4 nanocrystalline rods have been successfully synthesized for the first time by the colloidal hot-injection synthesis route and well-organized rod-like nanocrystals (NCs) with lengths ranging from 200 to 350 nm and widths from 10 to 30 nm were obtained. For this structure, the Ag_2MnSnS_4 exhibits a semiconductor property with a band-gap of approximately 1.3 eV. The optical properties and band-gap values were determined by UV-Vis absorption spectrum and using Tauc Equation. It has been observed that the Ag_2MnSnS_4 structure acquired by the proposed colloidal synthesis method can be an alternative to the commonly used materials based on Cd and Pb.

Key words: Ag_2MnSnS_4, AMTS, kesterite, nanorod, hot-injection

1. Introduction

Since the 20th century, the demand for energy sources has continuously increased due to technological developments and increasing demand in society. Currently, many studies are focused on finding solutions to generate alternative energy sources to meet the increasing energy demand. These studies present new possibilities for current-generation applications in hydrogen harvesting and storage, lithium-ion batteries, supercapacitors, solar cells, photodiode, and carbon dioxide reduction processes [1–6]. Efficiency and production costs have been crucial factors for the usability of energy applications. Therefore, the materials that have been used in energy applications must be cost-effective and efficient, as well as non-toxic [1–8]. Recently colloidal nanomaterials have given rise to an exceptional class of emissive materials in sensing and bio-imaging, owing to optical, high luminescence properties, and excellent processability. However, as Cd and Pb-based chalcogenides are the precursor materials in this field and are toxic heavy metals, their industrial spread might pose a threat to human health, which has led to the search for different alternatives. To ensure compliance with existing safety regulations RoHS (Restriction of Hazardous Substances), there has been a crucial need for the development of non(less)toxic colloidal nanocrystals. Pb/Cd-free, $((Ag,Cu)_2XSn(S,Se)_4$ X:Zn, Mn, Ni, Co) NCs produced by the hot injection synthesis route are non(less) toxic materials [9]. As an alternative to Cd and Pb-based chalcogenide materials, NIR-emitting indium/gallium-based group nanomaterials such as CuInGaS (CIGS), InSb, $GaAs_{7,}$ and $CuIn(S/Se)_2$, AgIn (Se/Te) have received attention. The need for alternative materials has continued to be examined because the lack of indium/gallium in the Earth's crust could limit large-scale commercial agreements. Recent studies showed that quaternary semiconductors of $((Ag, Cu)_2XSn(S,Se)_4)$ with a small band-gap, have shown NIR luminescence and are considered to be a potential alternative in this field of research [10,11]. The most interesting of these materials is Cu_2ZnSnS_4 (CZTS) NCs and it is shown as one of the energy materials of the future with its superior properties. CZTS NCs, which exhibit semiconductor properties, have direct band-gap properties and high absorption coefficients in the visible region ($\sim 10^4$ cm^{-1}). The band-gap of CZTS NCs has about 1.6–1.4 eV, which is close to the optimum value for solar cell application [12]. Compared to the CIGS structure, CZTS is non(less)toxic and the precursor elements are abundant on the earth (Zn and Sn are 1500 times and 45 times greater than that of In, respectively).

* Correspondence: farukozell@gmail.com

Recently, Ag_2XSnS_4 NCs, which have similar properties to CZTS NCs, have taken their place among the new remarkable structures in this field. In the literature review, only a few studies were found on the synthesis of Ag_2XSnS_4 NCs, and the details of these studies are given in the following lines. According to the study by Saha et al. they synthesized Ag_2ZnSnS_4 (AZTS) NCs by the colloidal synthesis technique. Their NCs were in a spherical shape with a 6 nm size and 1.5 eV band-gap [9]. In another report, Pietak et al. prepared high-quality AZTS NCs of various sizes with average band-gap energy of 2.0 eV by the chemical vapor transport (CVT) method [13]. Additionally, Kumar et al. reported that they produced the $(AgxCu_{1-x})_2ZnSnS_4$ (ACZTS) structure using the thin film method and ACZTS structure has different ratios (x:0–0.04) 1.6 eV, 2.4 eV band-gap respectively [14]. Amongst them, AMTS is one of the structures of recent interest as it demonstrates antiferromagnetic behaviors. However, an important limitation of the studies on AMTS mentioned is that solid-state and melt-annealing techniques requiring high temperature and complex processes are used for the synthesis of these structures [15,16].

In this study, AMTS nanorods (NRs) were obtained for the first time by the colloidal synthesis route, which is considered a more economical, Pb/Cd-free, and versatile route than previous techniques. Therefore, it is suitable for additive fabrication techniques such as printing and direct writing for large-scale or specific applications. The band-gap of obtained NRs by the proposed synthesis technique were calculated 1.3 eV. This indicates that AMTS NRs can be a promising absorbent material for energy conversion applications.

2. Experimental section

2.1. Materials

To perform experimental process, silver nitrate (AgNO3 99.99%), sulfur powder (99.5%), tin (II) acetate (Sn(OAc)2-99.99%), propanol (%99.5), ethanol (%99.8) were obtained from Sigma-Aldrich. Manganese (II) acetate (Mn(OAc)2-(%95) was purchased from Alfa-Aesar. Oleylamine (OAm %98.5), 1-Dodecantiol (DDT-%98), Ter-Dodecylmercatan (t-DDT) were purchased from Acros Organics. Toluene was provided by VWR.

2.2. Colloidal synthesis of AMTS NRs

AMTS NRs were synthesized by previously published CZTS nanocrystal synthesis methods with a small extent modification [10,17]. A schematic illustration of the production process is given in Figure 1a. Briefly, 0.5 mmol $AgNO_3$, 0.25 mmol $Mn(OAc)_2$, 0.25 mmol $Sn(OAc)_2$, and 15 mL OAm were added into a 50 mL three-neck flask and mixed under Ar gas flow, allowing the precursors to dissolve and the reaction medium to be deoxygenated. The reaction medium was heated until the solution temperature reached 100 °C, and at this temperature, 0.13 mL of DDT & 0.88 mL of the t-DDT mixture were injected into the solution. Afterward, the solution was instantly heated up to 240 °C and kept by stirring at this temperature for 30 min to complete the formation of the NRs. Fourteen mL of toluene and two mL of propanol were added to the obtained solution for particle formation and it was precipitated by centrifuging at 3000 rpm for 1 min. Finally, the resulting precipitate was washed with ethanol and left to dry.

2.3. Characterization

The surface morphology of as-prepared AMTS NRs was acquired by using the scanning electron microscope (SEM-Hitachi SU5000, Japan). The size distribution of the NRs and statistical data were analyzed by using the data program (Origin). The structure was analyzed via an X-ray diffractometer (Bruker D8, Germany) (CuKα source, λ = 1.5406 nm). Fast mapping and composition of the NRs have obtained SEM–EDS instruments (SEM–EDS Hitachi SU5000, Japan). The composition of AMTS NRs was analyzed by using an inductively coupled plasma-mass spectrometer (ICP-MS AGILENT 7500A, The United States). A confocal Raman microscope (Alpha 300 M+, WITec, Germany) was used for Raman spectrometry measurements. The morphology, crystalline structure, and size distribution were investigated using a transmission electron microscope (TEM) (JEOL JEM-2100F, Japan). The absorbance spectrum and optic band-gap of AMTS NRs were acquired and calculated by using a Shimadzu UV-3600 UV–vis–NIR spectrometer (Shimadzu UV-3600, Japan).

3. Result and discussions

The synthesis process of AMTS NRs was carried out in sequential and different processes. In the first step, the solution is formed by dissolving the precursor materials (Ag, Mn, Sn) in OLA. In the second step, the Ag_2S nucleus begins to form following the addition of the sulfur sources (DDT and t-DDT) in the synthesis medium (Figure 1a). Finally, by increasing the temperature, Mn and Sn atoms started to diffuse through the Ag_2S nucleus and the final rod particles were obtained by growing the nucleus with different chain structures of sulfur sources in the environment [18–21].

Figure 1b shows the EDS maps for the AMTS NRs. The mapping results bring to light that the elements in the AMTS structure are homogeneously distributed. According to the results of the EDS analysis, the atomic ratio of Ag, Mn, Sn, and S for the AMTS sample is estimated to be 0.38, 0.29, 0.28, and 1.05, respectively. These values are reasonably close to the ratios of 0.5, 0.25, 0.25, and 1 that are expected for the AMTS phase structure. The mean elemental composition (%) ratios of the NRs, given in Figure 1c, are close to the theoretical values. Also, the average composition of AMTS NRs was confirmed by ICP-MS as shown in Table. When the results are analyzed, it is clearly seen that the obtained values are quite close to the targeted composition value. In addition, the obtained results are compatible with the EDS results, confirming that the synthesized NRs have been successfully obtained.

It can be concluded from these results that it has been possible to obtain silver-based kesterite particles with nanorod structure by using the colloidal hot-injection method. Figure 1d shows the XRD pattern of the obtained NRs. The main diffraction peaks manifested themselves at about 2θ of 27.6°, 33.6°, 34.3°, 44.0°, 45.5°, 48.08°, 54.1°, and 56.4° which were assigned to (112), (004), (121), (220), (204), (301), (116), and (224) planes, respectively. The observed peak values agree with the tetragonal pirquitasite (JCPDS 35-435) structure. The unit cell of this structure consists of 23 polyhedra centered on Ag, Mn, and Sn atoms, and in this structure, each cation atom bonds with 6 sulfur atoms (Figure 1e). These results are consistent with previous reports conducted on AZTS and CZTS structures [9,22]. Moreover, diffraction peaks coming from the secondary Ag_2SnS_3 phase at 2θ: 28.9° and 41.5° can be identified and their attributes to (-202) and (-151) planes, respectively. The average crystallite size of obtained AMTS NCs has been calculated to be 23.3 nm using the Scherrer equation which is consistent with the particle widths observed by SEM (Figure 2a) and TEM (Figure 2b). Figure 2a and b present the typical SEM and TEM images of as-synthesized NRs. As shown in Figure 2 (a and b), the synthesized particles have mostly rod-shaped structures. It has been determined that the width of the particles varies between 10 to 30 nm, and the lengths vary between 200 to 350 nm. Figure 2 (c) shows a high-resolution TEM (HR-TEM) image of the NRs. The lattice fringe observed by the HR-TEM image is 0.33 nm, which corresponds to the (112) lattice plane of body-centered tetragonal AMTS (Figure 2c). Moreover, selected area electron diffraction (SAED) patterns of the NRs have been given in Figure 2d and indexed (112), (220), and (004) planes confirmed that the synthesized particles were in tetragonal-type of AMTS. The dotted structure is seen in the SAED pattern, which indicates a high degree of crystallinity and also confirms that the nature of the particles is single crystal. These results match the XRD and HR-TEM results.

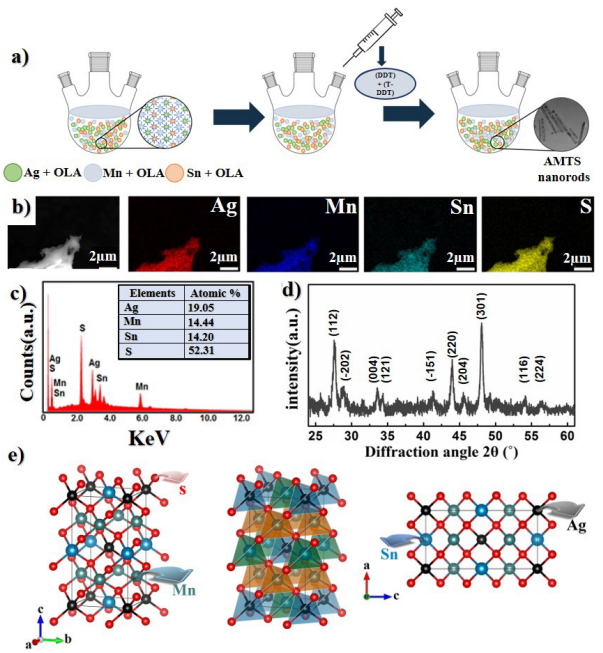

Figure 1. Schematic illustration of the colloidal synthesis of the AMTS NRs (a), EDS elemental mapping images (b), EDS spectrum (c) XRD pattern (d), and 3D-crystal structure (e) of the AMTS NRs.

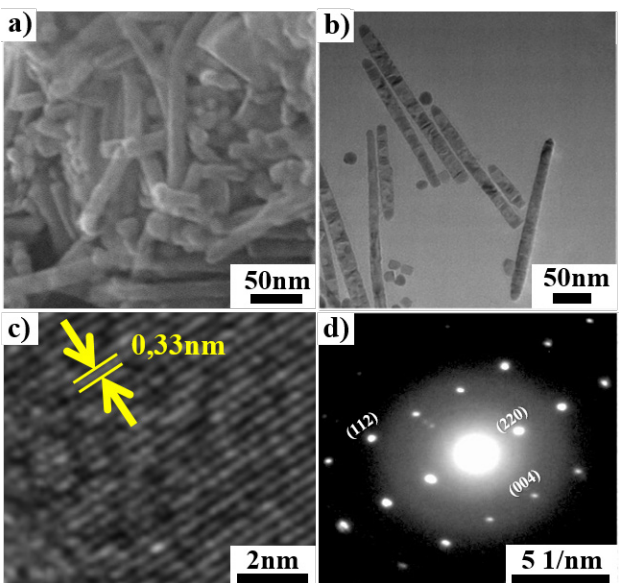

Figure 2. SEM image (a), TEM image (b), HR-TEM image (c), and SAED pattern (d) of AMTS.

Raman analysis was performed to determine the additional phase states that cannot be seen in XRD analysis. The Raman spectrum of the NRs (λexc = 514.7 nm) is shown in Figure 3. The spectrum exhibits a major peak at 337 cm^{-1} approximately, which is generally donated as the A_1 vibration mode which originates from the vibration of the sulfur sublattice [23,24]. Moreover, the NRs also exhibit peaks such as AMTS (337 cm^{-1}) [25], MnS (292 cm^{-1}) [26], and Ag_2SnS_3 (260 and 298 cm^{-1}) [27], all of which can be attributed to AMTS and all these peaks are in line with the reported results. Furthermore, the absence of any additional peaks from possible secondary phases also confirmed the purity of the synthesized NRs.

The optical properties, band-gap values, and species of the NRs were determined by using UV–vis absorption spectrum and diffuse reflection spectra. UV–vis absorption spectrum, diffuse reflection, and absorption spectra of the AMTS NRs are shown in Figure 4 (a, b). The optical band-gaps of these NRs were measured at around 1.3 eV by using Tauc Equation [28,29]. The obtained band-gap value is close to the optimal values reported in the literature for solar cell applications. For example; Li et al. have calculated $Cu_2ZnSn(S1-_xSex)_4$ NCs changing from 1.5 eV to 1.12 eV band-gaps [30], on the other hand, Su et al. have found CZTS nanowires and nanotubes 1.57 eV, 1.61 eV band-gaps respectively [31]. Also, Yıldırım et al. have determined 1.51 eV which is similar to the earlier report [32].

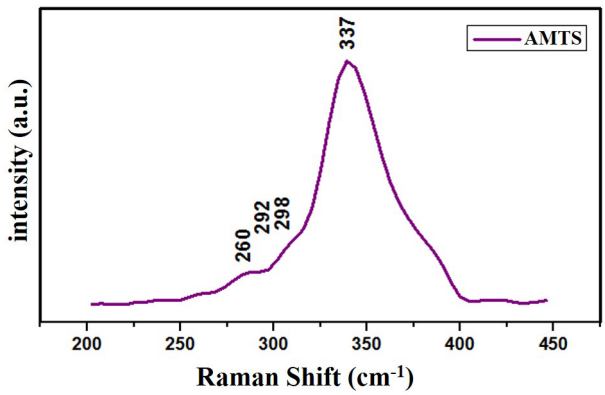

Figure 3. Raman spectrum of the AMTS NRs.

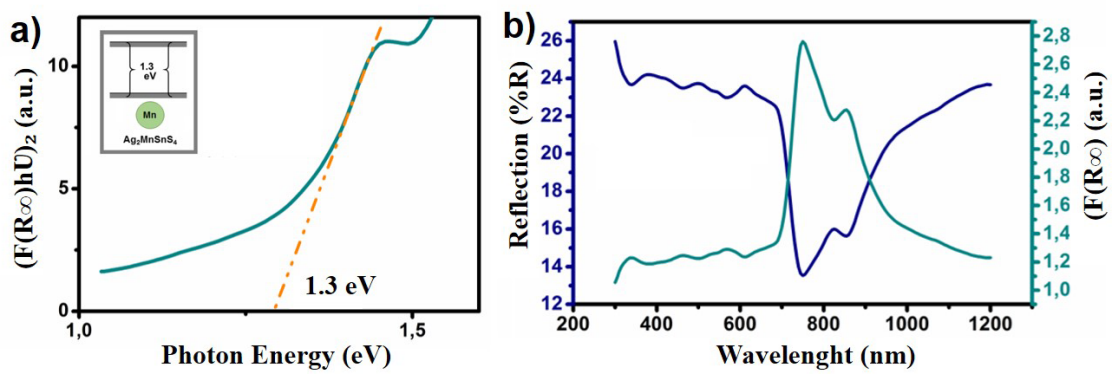

Figure 4. UV-vis and band-gap energy diagrams of the AMTS NRs (the inset shows the schematic illustration of calculated band-gap structure) (a) and diffuse reflection and absorption spectra (b).

Table. Composition of AMTS NRs measured ICP-MS.

Ag(%)	Mn(%)	Sn(%)	S(%)	Ag/(Mn+Sn)	Mn/Sn
22.4	13.2	12.9	51.5	~ 0.86	~ 1.0

4. Conclusion

In summary, colloidal AMTS NRs were successfully synthesized using a low-cost and facile colloidal hot-injection method. XRD, Raman, ICP-MS, and EDS measurements confirmed the stoichiometry of the AMTS structure. The morphology of the NRs was determined by SEM and TEM analysis, where the results show that the width varies between 10 to 30 nm, and the lengths vary between 200 to 350 nm. Moreover, HR-TEM and SAED images showed that the NRs are single crystalline. In conclusion, with this work, we demonstrate the first example of AMTS NRs by expanding the material availability of Pb/Cd-free colloidal nanoparticles.

Acknowledgment

We gratefully acknowledge the Scientific and Technological Research Council of Turkey (TÜBİTAK) for the financial support provided under project number 217M212. In addition, this paper is part of the MSc thesis prepared by Sultan Süleyman Özel.

References

1. Aslan E, Sarilmaz A, Yanalak G, Ozel SS, Ozel F et al. Transition metal–incorporated tungsten-based ternary refractory metal selenides (MWSex; M= Fe, Co, Ni, and Mn) as hydrogen evolution catalysts at soft interfaces. Materials Today Energy 2020; 18: 100510. doi: 10.1016/j.mtener.2020.100510
2. Bree G, Geaney H, Stokes K, Ryan KM. Aligned copper zinc tin sulfide nanorods as lithium-ion battery anodes with high specific capacities. Journal Physical Chemistry C 2018; 122: 20090–20098. doi: 10.1021/acs.jpcc.8b05386
3. Yu P, Zhang X, Chen Y, Ma Y. Solution-combustion synthesis of ε-MnO2 for supercapacitors. Materials Letters 2010; 64: 61–64. doi: 10.1016/j.matlet.2009.10.007
4. Wang W, Winkler MT, Gunawan O, Gokmen T, Todorov TK et al. Device characteristics of CZTSSe thin-film solar cells with 12.6% efficiency. Advanced Energy Materials 2014; 4: 1301465. doi: 10.1002/aenm.201301465
5. Yıldırım, M, Kocyigit, A, Sarilmaz, A, Ozel SS, Kus M et al. Ternary CuCo2S4 Thiospinel Nanocrystal-Coated Photodiode with Improved Photoresponsivity and Acceptance Angles for Optoelectronic Applications. Journal of Electronic Materials 49, 949–958 (2020). doi: 10.1007/s11664-019-07841-z
6. Coskun H, Aljabour A, De Luna P, Farka D, Greunz T et al. Biofunctionalized conductive polymers enable efficient CO2 electroreduction. Science Advances 2017; 3 (8): e1700686. doi: 10.1126/sciadv.1700686
7. Coughlan C, Ryan KM. Complete study of the composition and shape evolution in the synthesis of Cu2ZnSnS4 (CZTS) semiconductor nanocrystals. CrystEngComm 2015; 17: 6914–6922. doi: 10.1039/C5CE00497G
8. Fan FJ, Wu L, Gong M, Chen SY, Liu GY et al. Linearly arranged polytypic CZTSSe nanocrystals. Science Reports 2012; 2: 1–6. doi: 10.1038/srep00952
9. Saha A, Figueroba A, Konstantatos G. Ag2ZnSnS4 Nanocrystals Expand the Availability of RoHS Compliant Colloidal Quantum Dots. Chemistry of Materials 2020; 32: 2148–2155. doi: 10.1021/acs.chemmater.9b05370
10. Saha A, Konstantatos G. Ag2ZnSnS4–ZnS core–shell colloidal quantum dots: a near-infrared luminescent material based on environmentally friendly elements. Journal of Material Chemistry C 2021; 9: 5682–5688. doi: 10.1039/D1TC00421B
11. Sarilmaz A, Ozel F. Synthesis of band-gap tunable earth-abundant CXTS (X= Mn+2, Co+2, Ni+2 and Zn+2) NCs: Toward a generalized synthesis strategy of quaternary chalcogenides. Journal of Alloys and Compounds 2019; 780: 518–522. doi: 10.1016/j.jallcom.2018.11.370
12. Zhou YL, Zhou WH, Li M, Du YF, Wu S. "Hierarchical Cu2ZnSnS4 particles for a low-cost solar cell: morphology control and growth mechanism." The Journal of Physical Chemistry C 2011; 115 (40): 19632-19639. doi: 10.1021/jp206728b
13. Pietak K, Jastrzebski C, Zberecki K, Jastrzebski DJ, Paszkowicz W et al. Synthesis and structural characterization of Ag2ZnSnS4 crystals. Journal of Solid State Chemistry 2020; 290: 2–7. doi: 10.1016/j.jssc.2020.121467
14. Kumar J, Ingole S. Optical phonons in pentanary compound (AgxCu1− x)2ZnSnS4 semiconductor: A raman study. Journal of Alloys and Compounds 2021; 865: 158113. doi: 10.1016/j.jallcom.2020.158113
15. Delgado GE, Sierralta N, Quintero M, Quintero E, Moreno E et al. Synthesis, structural characterization and differential thermal analysis of the quaternary compound Ag2MnSnS4. Revista Mexicana de Fisica 2018; 64: 216–221.
16. Friedrich D, Greil S, Block T, Heletta L, Pöttgen R et al. Synthesis and Characterization of Ag2MnSnS4, a New Diamond-like Semiconductor. Zeitschrift für Anorganische und Allgemeine Chemie 2018; 644: 1707–1714. doi: 10.1002/zaac.201800142
17. Singh A, Geaney H, Laffir F, Ryan KM. Colloidal Synthesis of Wurtzite Cu2ZnSnS4 NCs and Their Perpendicular Assembly. Journal of American Chemical Society 2012; 134(6): 2011–2014. doi: 10.1021/ja2112146

18. Ha E, Lee LYS, Man HW, Tsang SCE, Wong KY. Morphology-controlled synthesis of Au/Cu2FeSnS4 core–shell nanostructures for plasmon-enhanced photocatalytic hydrogen generation. ACS Applied Materials Interfaces 2015; 7: 9072–9077. doi: 10.1021/acsami.5b00715

19. Connor ST, Hsu C M, Weil BD, Aloni S, Cui Y. Phase transformation of biphasic Cu2S–CuInS2 to monophasic CuInS2 nanorods. Journal of American Chemical Society 2009; 131: 4962–4966. doi: 10.1021/ja809901u

20. Kruszynska M, Borchert H, Parisi J, Kolny-Olesiak J. Synthesis and shape control of CuInS2 nanoparticles. Journal of American Chemical Society 2010; 132: 15976–15986. doi: 10.1021/ja103828f

21. Zhang X, Xu Y, Pang C, Wang Y, Shen L et al. Insight into the crystal phase and shape evolution from monoclinic Cu1.94S to wurtzite Cu2ZnSnS4 nanocrystals. CrystEngComm 2018; 20: 2351–2356. doi: 10.1039/C8CE00048D

22. Mkawi EM, Ibrahim K, Ali MKM, Mohamed AS. Dependence of copper concentration on the properties of Cu2ZnSnS4 thin films prepared by electrochemical method. International Journal of Electrochemical Science 2013; 8: 359–368.

23. Himmrich M., Haeuseler H. Far infrared studies on stannite and wurtzstannite type compounds. Spectrochimica Acta Part A: Molecular Spectroscopy. 1991; 47(7), 933-942. doi: 10.1016/0584-8539(91)80283-O

24. Ozel F, Aslan E, Istanbullu B, Akay O, Patir IH. Photocatalytic hydrogen evolution based on Cu2ZnSnS4, Cu2NiSnS4 and Cu2CoSnS4 nanocrystals. Applied Catalysis B: Environmental 2016; 198, 67-73. doi: 10.1016/j.apcatb.2016.05.053

25. Friedrich D, Greil S, Block T, Heletta L, Pöttgen R et al. Synthesis and Characterization of Ag2MnSnS4, a New Diamond-like Semiconductor. Zeitschrift für anorganische und allgemeine Chemie 2018; 644 (24): 1707-1714. doi: 10.1002/zaac.201800142

26. Chen L, Deng H, Tao J, Cao H, Sun L et al. Strategic improvement of Cu2MnSnS4 films by two distinct post-annealing processes for constructing thin film solar cells. Acta Materialia 2016; 109, 1-7. doi: 10.1016/j.actamat.2016.02.057

27. Chen L, Deng H, Tao J, Cao H, Huang L et al. Synthesis and characterization of earth-abundant Cu2MnSnS4 thin films using a non-toxic solution-based technique. RSC advances 2015; 5 (102): 84295-84302. doi: 10.1039/C5RA14595C

28. Le T.L, Guillemet-Fritsch S, Dufour P, Tenailleau C. Microstructural and optical properties of spinel oxide MxCo2 - XMnO4 (M = Ni, Zn or Cu; 0 < x < 1) thin films prepared by inorganic polycondensation and dip-coating methods. Thin Solid Films 2016; 612: 14–21. doi: 10.1016/j.tsf.2016.05.030

29. Sarilmaz A, Yanalak G, Aslan E, Akyildiz H, Patir IH et al. Ternary and quaternary thiospinel nanocrystals with adjustable compositions: effects of Band-Gaps and nanostructures on Visible-Light-Driven photocatalytic H2 evolution. Materials Today Energy 2020; 16: 100413. doi: 10.1016/j.mtener.2020.100413

30. Ji S, Shi T, Qiu X, Zhang J, Xu G et al. A route to phase controllable Cu2ZnSn(S1−xSex) 4 nanocrystals with tunable energy bands. Science Reports 2013; 3: 1–7. doi: 10.1038/srep02733

31. Su Z, Yan C, Tang D, Sun K, Han Z et al. Fabrication of Cu2ZnSnS4 nanowires and nanotubes based on AAO templates. CrystEngComm 2012; 14: 782–785. doi: 10.1039/C2CE06236D

32. Yıldırım M, Ozel F, Tugluoglu N, Yuksel OF, Kus M. Optical characterization of Cu2ZnSnSe4-xSx nanocrystals thin film. Journal of Alloys Compounds 2016; 666: 144–152. doi: 10.1016/j.jallcom.2016.01.107